Fine structure of streamer-to-filament transition in high-pressure nanosecond surface dielectric barrier discharge

Ch Ding, A Jean, N A Popov, S M Starikovskaia

Fine structure of streamer-to-filament transition in high-pressure nanosecond surface dielectric barrier discharge

Ch. Ding, A. Jean, N. A. Popov, S. M. Starikovskaia

Laboratory of Plasma Physics (CNRS, Ecole Polytechnique, Univ. Paris-Sud, Observatoire de Paris, Sorbonne Université, l'Institut Polytechnique de Paris), Ecole Polytechnique, route de Saclay, 91128 Palaiseau, France

E-mail: svetlana.starikovskaia@lpp.polytechnique.fr

Abstract. The fine structure of a streamer–to–filament transition in a single–shot high–voltage nanosecond surface dielectric barrier discharge (nSDBD) in molecular nitrogen at pressure $P = 6$ bar was studied with the help of ICCD microimaging. An intermediate discharge structure, existing for only a few nanoseconds, was observed in the time interval between two discharge modes: streamer discharge, with a typical electron density of $n_e \sim 10^{15}$ cm^{-3}, and filamentary discharge, with $n_e \sim 10^{19}$ cm^{-3}. The structure was observed for both polarities of the high–voltage electrode. The structure can be briefly described as a stochastic appearance of thin channels propagating a bit faster than the main ionization front of merged surface streamers, transforming in a few nanoseconds in a bi–directional ionization wave. One wave, which we associate with a feather–like structure in optical emission, propagates further away from the high–voltage electrode, and another, a backward wave of emission, propagates back towards the edge of the high–voltage electrode. When the backward wave of emission almost reaches the high–voltage electrode, the filament appears. Plasma properties of the observed structure were studied to better understand the nature of a streamer–to–filament transition. Theoretical analysis suggests that the instability of a flat front of ionization wave (Laplacian instability) triggers the streamer–to–filament transition, and that a surface stem (a tiny region with enhanced electron density) should be in the origin of the bi-directional ionization wave.

Keywords: streamer–to–filament transition, nanosecond surface dielectric barrier discharge, micro–scale, bi–directional ionization wave

Introduction

For over a century [1, 2], research in the field of dielectric barrier discharges (DBDs) has been supported by various applications. According to different electrode configurations, DBDs can be divided into volume discharges, surface discharges and coplanar discharges [3]. Already implemented and in development applications of DBDs include plasma catalysis [4], air pollution control [5–7], light source generation [8, 9], materials processing for microelectronics and photovoltaic cells [10], medical equipment disinfection [11], plasma–assisted flow control [12–14], plasma–assisted ignition and combustion [15–18], etc.

Studying high–pressure discharges for the needs of plasma-assisted ignition, it was found [19] that, with an increase in pressure and/or voltage, the nanosecond surface dielectric barrier discharge (nSDBD) transforms from a streamer mode, typical for ambient conditions, into a filamentary mode. As a result, starting with a streamer mode, the discharge transforms into a set of filaments, separated by a distance of ∼1 mm or less, propagating away from the high–voltage electrode. This streamer–to–filament transition was observed in single–shot experiments for a wide range of pressures [19] and gas mixtures [20, 21], on different dielectrics and different electrode materials [22]. At the moment of transition, during $1-2$ nanoseconds, the emission spectrum changes from streamer–like emission, containing mainly the molecular bands of N_2, to the continuous wavelength (*cw*) emission with well distinguished broadened lines of neutral (N, O, H) and singly ionized atoms, mainly N^+. The continuous wavelength emission comes from the narrow near–axis zone of the filament. The electron density during the transition increases, during a few nanoseconds, from $n_e \sim 10^{15}$ cm^{-3} to $n_e \sim 10^{18} - 10^{19}$ cm^{-3}, and then a slow decay of the electron density, a few tens of nanoseconds long, is observed. The specific delivered energy is extremely high for the filamentary mode, more than 5 eV/particle [23], and does not depend upon applied voltage. According to theoretical consideration and numerical modeling [23], complete or almost complete dissociation, and plasma close to local thermal equilibrium (LTE) conditions, are achieved in the filaments.

It should be noted that fast transition from low to high electron density and similar plasma parameters were also observed in bulk nanosecond discharges [24–27]. Work that was "ahead of its time" are the articles [24,25] published in 1977. In 1977, Stritzke *et al.* [24] made spatial and temporal spectroscopy measurements on the streamer–to–spark transition in nitrogen (0.4 bar) on a plane-to-plane electrode system with a 2 cm gap. They observed the second positive system of molecular nitrogen (SPS), N_2 ($C^3\Pi_u \rightarrow B^3\Pi_g$) in the emitted light. The electron density was found to be increasing from 10^{11} cm^{-3} to 10^{16} cm^{-3} with the heating of the plasma channel. A few nanoseconds after closing the gap, intense dissociation and ionization provided a strong continuum emission as well as a few atomic lines in the wavelength range of $300 - 860$ nm. At this stage, the electron temperature reached $(5 - 6) \times 10^4$ K and the electron density increased up to 10^{18} cm^{-3}. Finally, the authors concluded that a LTE state had been

established in the ionized plasma channel. The same year, Albrecht *et al.* [25] made a series of experiments on the spark discharge to study the combustion of fuel:air mixtures at atmospheric pressure. They reported that the SPS emission, peaking at 337.1 nm, was observed only at the beginning of the discharge and disappeared rapidly when closing the gap. After rising of the current, the atomic lines NII (N^+), peaking at 500.6 nm, as well as the radiation of electrode material (MnII (Mn^+)), peaking at 230.3 nm, are generated within a few nanoseconds, accompanied by the constriction of discharge channel. The full ionized channel has a width of a few tens of micrometers. The electron density at the thermodynamic equilibrium state was measured by the Stark broadening and reported to be as high as 10^{19} cm^{-3}. The electron temperature was calculated from the Boltzmann plot of N^+ lines and was over 5 eV.

The effect of the rapid, nanosecond, or even sub-nanosecond, transition from streamer–like to the arc–like plasma has been reinvented in the last decade, while investigating the properties of short pulsed nanosecond discharges [26–28]. This type of discharge, obtained with pulses of a few tens of nanoseconds, was called a thermal spark [27]. Lomaev *et al.* [29] observed the constriction of plasma when increasing the pressure from $0.1 - 4$ bar to over 5 bar. In their experiments, a steel tube, 6 mm in diameter and 50 μm thick, served as the cathode, while a flat brass plate was used as the anode. The length of the discharge gap was 12 mm. The homogeneous diffuse plasma filled the volume between the cathode tube and the anode at lower pressure conditions ($0.1 - 4$ bar). As the experiments were conducted in nitrogen with 5% of hydrogen, the strong emission of the SPS of molecular nitrogen appeared during the homogeneous discharge regime. When pressure reached 6 bar, a broadband continuum spectrum in the wavelength range of $200 - 800$ nm appeared, as well as NI (N atom) and NII atomic lines in the range of $400 - 800$ nm. With the continuous increase of pressure from 6 bar to 12 bar, the emission intensity of atomic lines and continuum spectrum grew significantly. The contraction of the discharge channels was accompanied by a significant increase in the electron density, from 10^{15} cm^{-3} in diffuse mode to 10^{17} cm^{-3} in contracted discharge. High electron temperature, up to 3.5 eV, was observed after the breakdown happened in the gap, and dropped rapidly to ~ 2 eV in a few nanoseconds.

Similar constriction of discharge channels was reported by Shao *et al.* in [28] where a tube–to–plane electrode configuration was used. They saw a contraction of the discharge channels when increasing the gas pressure or shortening the gap between the electrodes. At the initial stage, before the transition, there were a few spots on the cathode. A few nanoseconds later, the spark channels was first generated on the anode and propagated towards the middle of the gap. The authors believed that it was the propagation of the spark leaders from the anode that bridged the discharge gap. Analogously, the spectra before breakdown were dominated by the SPS of molecular nitrogen, while after the gap was bridged, mainly the continuum and NII, NI and OI (O atom) spectra, as well as the atomic lines from electrode materials, were observed.

Nanosecond repetitive pulsed (NRP) discharge at atmospheric pressure in sub-millimeter gaps (0.1-1 mm) was studied by Orriere *et al.* [26, 30]. The authors showed a

sharp increase of the electron density to 1×10^{19} cm^{-3}, corresponding to an ionization fraction of air of 0.5. After reaching its maximum value, n_e decayed slowly with a characteristic recombination time of ~ 90 ns. This is consistent with a slow relaxation of the electron temperature T_e and the nearly complete ionization and dissociation of the gas in the microplasma. The electron temperature was measured to be 72 kK at 5 ns after the end of the voltage pulse.

Minesi *et al.* [27] very recently observed the formation of highly ionized plasma channels in experiments performed at pressures ranging from 58 mbar to 1 bar. After ignition of the discharge, a diffuse plasma was generated between anode and cathode within 1.25 ns and first appeared near the anode. Then, a filament with higher emission intensity originated on the edge of the cathode within 1 ns. Because of limitations of the ICCD camera, the authors were not able to resolve the appearance of the filament. Immediately after, the fully ionized filamentary discharge also appeared on the anode. Finally, as a result of the continuous propagation of filaments from both cathode and anode to the middle of the gap, the discharge channel closed the gap between two electrodes a few nanoseconds after the ignition. When the breakdown happened in the gap, the electron temperature was as high as 4.1 eV and the peak electron density was equal to 4×10^{19} cm^{-3}. The authors suggested four different stages of the NRP discharge development as a function of specific delivered energy, namely NRP–corona, NRP–glow, NRP–spark and NRP–thermal spark. The NRP–thermal spark in pin–to–pin geometry is very similar in parameters to filaments in nSDBD discharge.

A distinctive feature of filamentation in SDBD is that, unlike a single plasma channel formed in volume discharges [24–27], a streamer–to–filament transition in SDBDs always occurs in a multichannel mode and is accompanied by a sharp decrease in the number of plasma channels observed in the streamer form before the transition. In addition, the transition to the NRP-thermal spark mode is observed when the primary streamer channel has already crossed the gap, while in SDBD there is no gap closure. Based on this, it should be expected that some important features of the SDBD filamentation mechanism differ significantly from the mechanism of thermal spark formation in single channel volume discharges.

No convincing theoretical model of streamer–to–filament transition in SDBD exists for the moment. It should be noted that the problem is essentially 3-dimensional. Recently, propagation of nSDBD streamers in high-pressure air ($P = 6$ atm), under conditions close to the experiments of the present paper, was studied numerically [31]. A high-pressure positive streamer was simulated, using a 2D approximation, up to the moment corresponding to streamer–to–filament transition in experiments. Secondary ionization waves were observed: they formed near the high-voltage electrode (anode) and propagated along the dielectric surface in the immediate vicinity of this surface, at a distance of less than 10 μm. The reason for the formation of such secondary ionization waves is not yet fully understood, but they hardly can be the origin of the streamer-to-filament transition. Indeed, it was experimentally shown that transition to the filamentary mode of nSDBD [23] or to the thermal spark mode of volumetric

discharge [27] requires a very high ionization degree, capable of initiating the transition of the discharge to the LTE mode. At the same time, the appearance of secondary ionization waves near the dielectric surface in simulations [31] occurred in regions where the electron density was extremely low, which makes the transition to the LTE state extremely unlikely within the physical model [31].

The aim of this work is to study in detail the features of the streamer–to–filament transition in high pressure nSDBD at positive and negative polarity: the morphology of the discharge before and after the transition, typical dimensions of plasma channels and, most importantly, find the point of origin of the filament.

1. Experimental setup

The coaxial electrode system is presented in figure 1 (a) and described elsewhere [20,21,23,32]. A metal disc, 20 mm in diameter, served as a high–voltage (HV) electrode. For the set of experiments on optical emission spectra, the disc has been purposely replaced by a same diameter gear. The internal diameter of the low–voltage grounded electrode was equal to the diameter of the high–voltage electrode, and the external diameter of the low–voltage electrode was equal to 50 mm. A thin 0.3 mm dielectric layer (PVC, $\varepsilon \approx 3 - 3.5$) was glued to the grounded electrode by Geocel FIXER Mate silicon glue ($\varepsilon \approx 3$). The thickness of the glue layer was 0.3 ± 0.1 mm, giving a total thickness for the dielectric of 0.6 ± 0.1 mm.

The electrode system was mounted into a constant–volume high–pressure chamber having 3 quartz optical windows of 5 cm diameter each (see figure 1 (b)). One optical window was situated in front of the electrode. The images of the discharge, as well as the optical emission spectra, were acquired through the front window. Two other windows allowed the observation of the discharge from the side.

The discharge chamber was pumped down to $\sim 10^{-3}$ Torr before the experiments; molecular nitrogen (Air Liquide) with < 100 ppm of impurities was used. The experiments were performed in a single–shot regime at ambient initial temperature. In particular cases when accumulation of the signal was needed, the repetitive frequency of the discharge did not exceed 1 Hz.

The images ($\lambda = 250 - 800$ nm) were taken by a Pi-Max4 Princeton Instruments ICCD camera. Optical emission spectra in the range 300-700 nm were recorded by an ACTON spectrometer (SP-2500i, 600 I/mm and 1200 I/mm gratings) and the ICCD camera. The synchronization of the ICCD camera was provided by the signal from a special back current shunt [33] soldered in the shielding of the high-voltage cable 1 m apart from the high-voltage generator. The accuracy of synchronization of the high-voltage signal coming to the electrode and ICCD camera was within 0.2 ns.

A Long distance microscope QM1 LDM (LaVision) was used to observe the discharge at a micrometer scale. The LDMs, widely used in combustion research, allow a high magnification and resolution while maintaining low aberrations and a long working distance, $52 - 180$ cm in our case. By working principle, the QM1 LDM is a Maksutov-

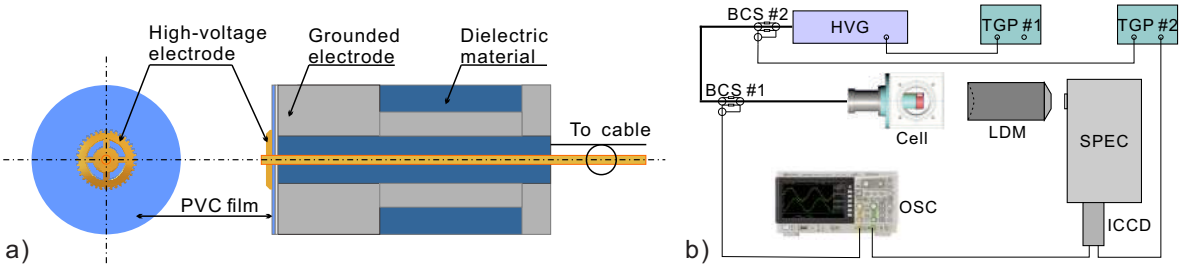

Figure 1. (a) Electrode system and (b) experimental setup. HVG — high-voltage generator, BCS — back current shunt, TGP — triggering generator, LDM — long distance microscope, SPEC — spectrometer, ICCD — intensified CCD camera, OSC — oscilloscope.

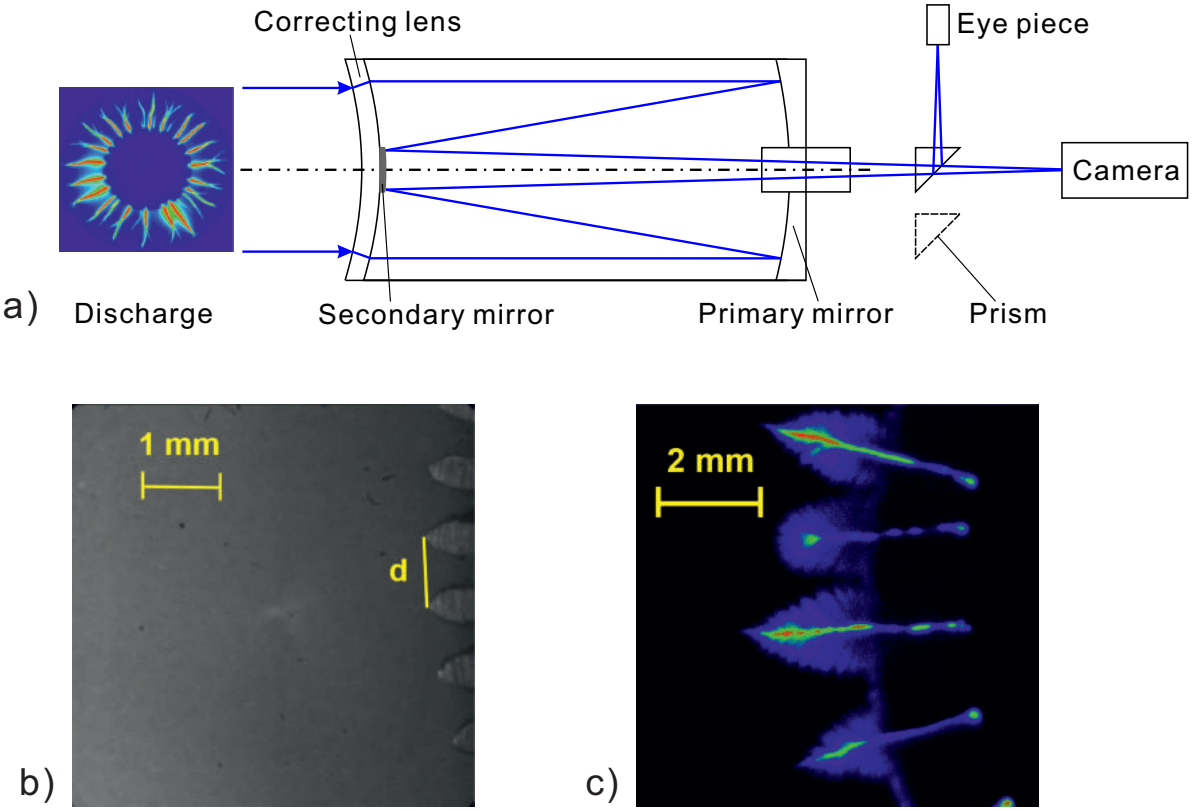

Figure 2. (a) Working principle of LDM imaging; (b) an example of micro–image of the edge of the gear-shaped electrode. $d = 0.9$ mm; (c) an example of micro–image of the nSDBD discharge.

Cassegrain catadioptric telescope, the scheme of which is presented in figure 2 (a). A typical depth of field with standard optics comprises part of a millimeter (800±30 μm for the focal distance 52 cm). When needed, one or more Barlow lenses (a concave diverging lens that increases artificially the focal distance of the optical setup) were added between the LDM and the ICCD to achieve a higher magnification. The best resolution achieved by the system was $1.1 - 2$ μm/pxl, depending upon the focal distance. A part of the gear–shaped high–voltage electrode is shown in figure 2 (b). The image was taken with

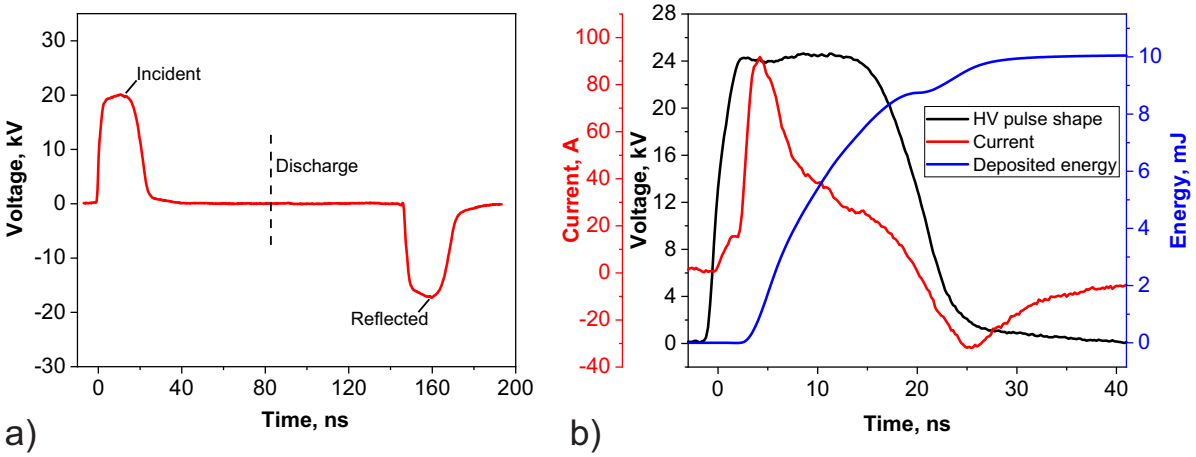

Figure 3. Typical electrical characteristics measured by BCS#1. (a) incident and reflected voltage waveforms; (b) synchronized voltage, current and deposited energy.

one Barlow lens; the resolution is 5 μm/pxl. The distance between the gear teeth is equal to $d = 0.9$ mm. In this work, most of the data were obtained without Barlow lens, with a resolution of 7.6 μm/pxl and a focal distance of 100 cm. The direction of observation was perpendicular to the surface of the dielectric.

Voltage and current were monitored in each experiment. The voltage waveforms were obtained with the help of a calibrated back current shunt BCS#1 installed in the middle of the cable, the technique is described in details elsewhere [34]. Current through plasma was calculated subtracting the capacitive current from the total current measured by the back current shunts. The capacitive current was measured experimentally at the conditions when the discharge is absent, similar to [19, 32].

Positive or negative polarity high–voltage pulses were delivered by a 30 m long coaxial 50 Ω cable connecting the high pressure chamber and the FPG20-03PM or FPG20-03PN pulsers (FID GmbH). These pulses were identical in shape, had a 20 ns duration, 2 ns rise time and an amplitude of $25-45$ kV on the high voltage electrode. A typical waveform of the voltage halfway of the cable (at the position of the BCS#1) is given in figure 3 (a). Typical time–synchronized voltage on the high voltage electrode, plasma current, and energy deposited in the gas during the discharge, are shown in figure 3 (b).

2. Selection of the experimental conditions

To select the experimental conditions properly, a special set of images with a high spatial resolution (7.6 μm/pxl) has been taken. The results were compared with the previous data on streamer–to–filament transition [21]. The data were taken for negative (figure 4) and positive (figure 5) polarities of the discharge, for a disk–shaped high–voltage electrode with a smooth edge, and for a gear–shaped electrode. For the whole set of experiments, the ICCD camera gate was equal to 1 ns, and the time delay from

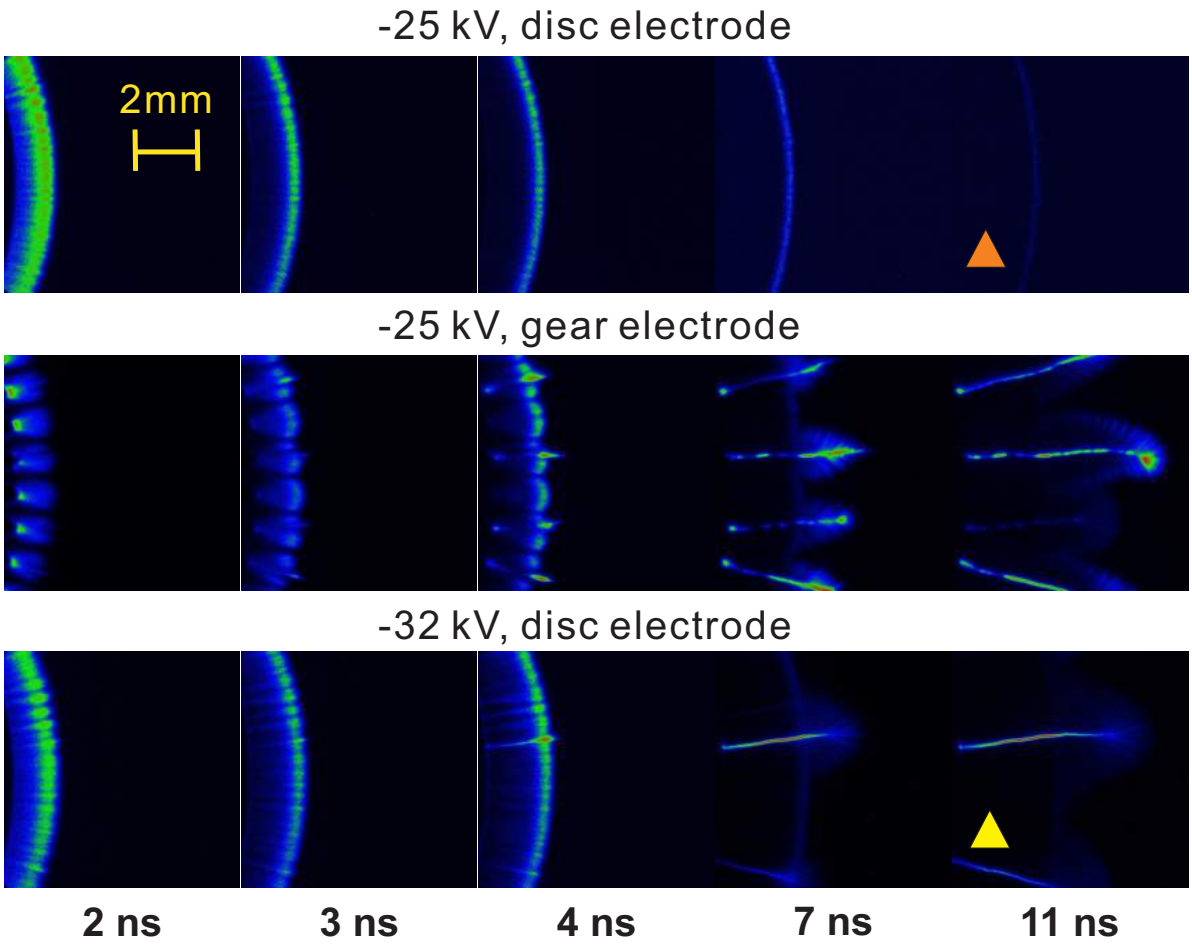

Figure 4. Micro–images of streamer-to-filament transition at negative polarity; nSDBD in 6 bar nitrogen. ICCD gate is 1 ns. For orange and yellow triangles see explanation in the text.

the beginning of the discharge was progressively increased with a step of 1 ns. The time instants are indicated below the frames.

It is clearly seen that for both types of electrodes, the picture of transition is similar qualitatively, the voltage of transition being slightly lower for the gear–shaped electrode. At 11 ns, for the electrode with a smooth edge, the discharge stays a streamer discharge at a voltage amplitude on the electrode of $U = \pm 25$ kV, and well–developed filaments are observed for $U = \pm 32$ kV. Corresponding frames are marked with orange and yellow triangles respectively. When using the gear–shaped electrode the transition voltage is lowered, the filaments are already observed at $U = \pm 25$ kV, but the general picture of the streamer–to–filament transition remains the same.

Figure 6 summarizes the transition curves for nitrogen in the system with the smooth–edge electrode. The transition curves were obtained by ICCD imaging of the discharge with a 12 ns gate starting at the beginning of the discharge. While varying the pressure and voltage gradually, we analyzed the ICCD images obtained. The transition point was defined when 3 to 5 filaments started to appear. The transition

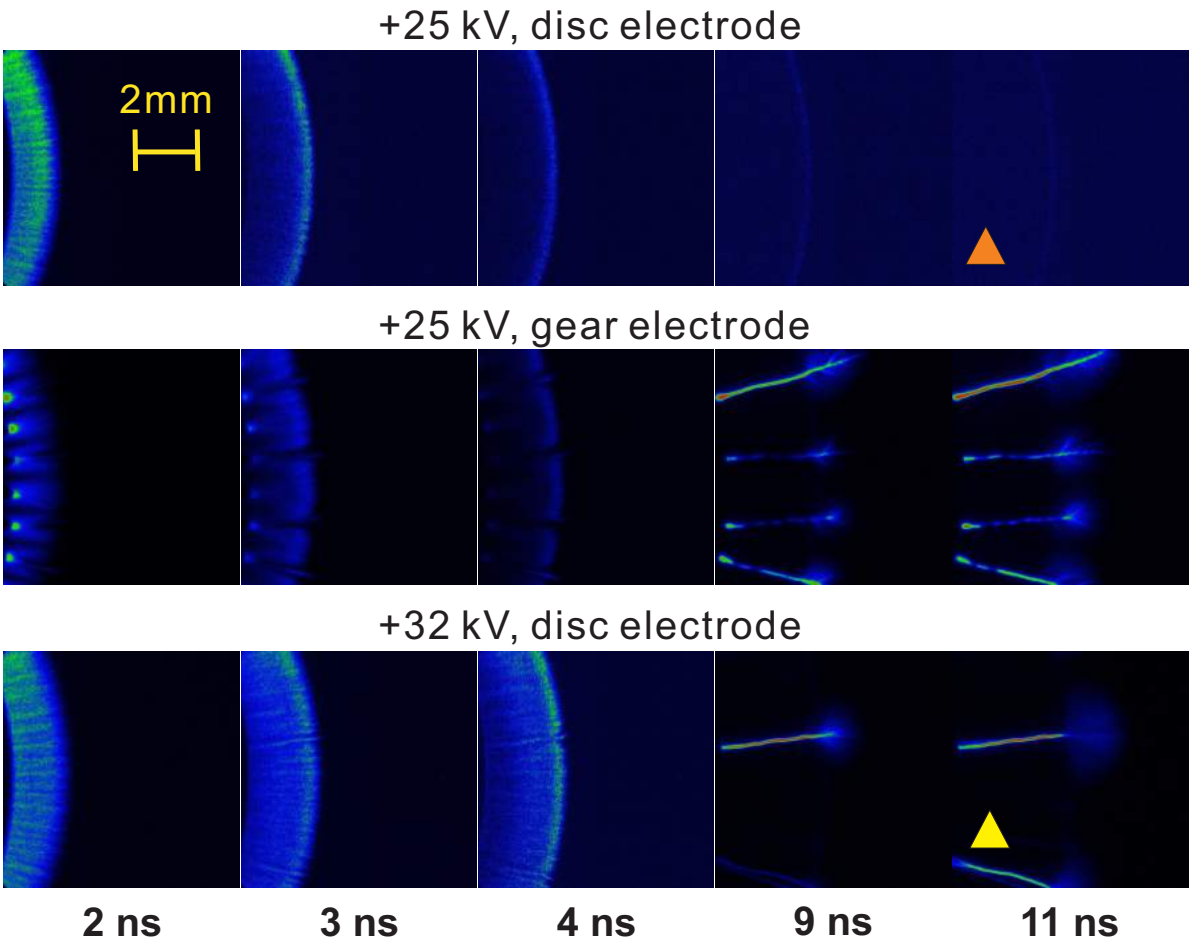

Figure 5. Micro–images of streamer-to-filament transition at positive polarity; nSDBD in 6 bar nitrogen. ICCD gate is 1 ns. For orange and yellow triangles see explanation in the text.

curves for both polarities intersect at the point $P = 6$ bar, the transition voltage being around $U_{tr} = \pm 30$ kV. Orange and yellow triangles indicate conditions similar to the corresponding frames in the figures 4, 5.

Aiming to change the minimum number of parameters from experiment to experiment, we have chosen pressure $P = 6$ bar as the base one. Since it was necessary to fix the starting point of the plasma channel for carrying out spectroscopic studies, the gear electrode was used in further experiments. For all the experiments presented in this work, it was verified that the results remain qualitatively the same in the case of a discharge starting from the smooth edge or the disk–shaped electrode.

3. Results and discussion

The following experiments have been made at a micro–scale for a streamer-to-filament transition:

- spectral analysis of optical emission for N_2 at 6 bar and $U = -25$ kV — figures 7, 8;

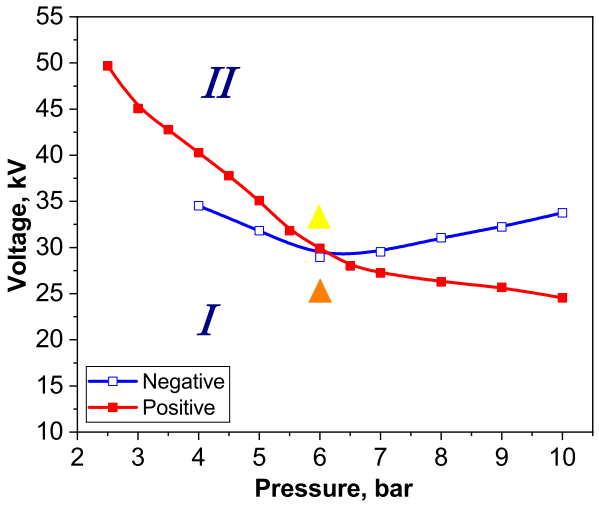

Figure 6. Curves of streamer-to-filament transition taken for the discharge in N_2 starting from the disk electrode with the smooth edge at the condition that the transition happens during the first 12 ns of the discharge. *I* is a region where streamer discharge is developed; *II* is a region where filamentary discharge is developed. For orange and yellow triangles see explanation in the text.

- detailed structure, or "morphology" of plasma during the transition for N_2 at 6 bar and $U = \pm 25$ kV — figure 9;
- diameter of a plasma channel (streamer, later filament) N_2 at 6 bar and $U = -25$ kV and $U = -32$ kV — figures 10, 11;
- $x - t$ diagrams of separate plasma structures observed at a micro–scale (for the conditions of figure 9) during the transition — figure 12;
- 3D distribution in time and space (for the conditions of figure 9) of optical emission integrated in wavelength — figure 13;
- Analysis of the "point of origin" of a high electron density, namely of the FWHM of H_α emission (5% H_2 in N_2, 6 bar and $U = -32$ kV) along the discharge channel at different time instants — figure 14;
- Analysis of the "point of origin" of the filament, namely of the distribution of excited atoms of hydrogen (5% H_2 in N_2, 6 bar and $U = -32$ kV) and the intensity of filament-like emission (N_2, 6 bar and $U = -25$ kV) along the discharge channel at different time instants — figure 15.

3.1. Spectral analysis of optical emission

Time–resolved, over the wavelength integrated ICCD micro–images, for the period $t = 2 - 12$ ns from the start of the discharge, were obtained through the slit of the spectrometer in zero order of a diffraction grating (figure 6). The direction of collection of radiation is perpendicular to the surface of the dielectric. The discharge

propagates from the high–voltage (HV) electrode along the grounded electrode covered with dielectric. In this section, as the tooth of the HV electrode has been put at the top of the slit, the discharge propagates vertically, from the top of the image to the bottom. The experiments were performed in 6 bar nitrogen at negative polarity ($U = -25$ kV).

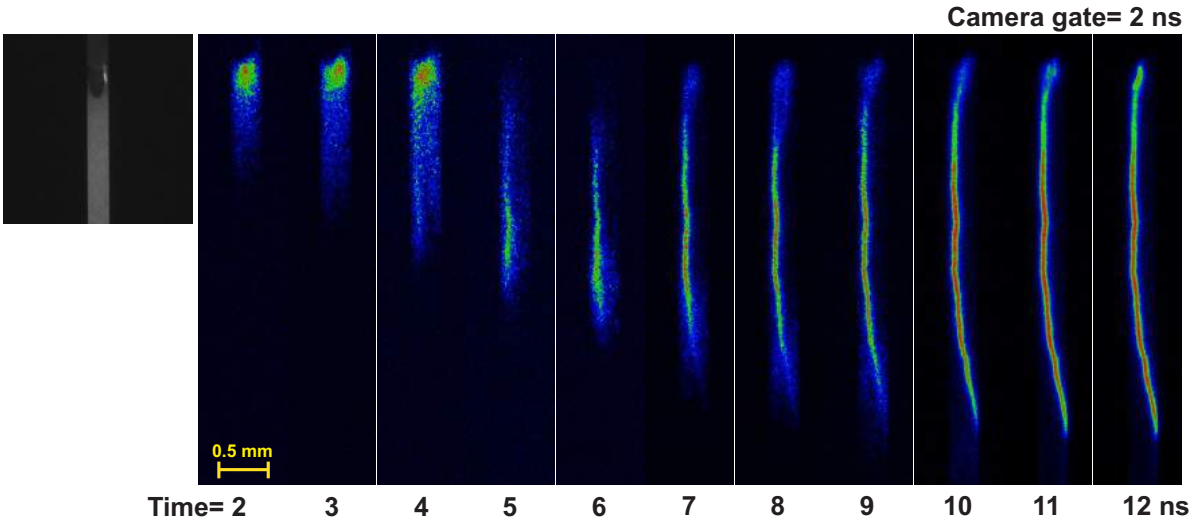

Figure 7. Time–resolved micro–images of discharge propagation in the time interval $t = 2 - 12$ ns measured by zero order of gratings through the slit of the spectrometer. $U = -32$ kV, 6 bar, N_2/H_2 (5%), ICCD camera gate 2 ns, 10 accumulations/image.

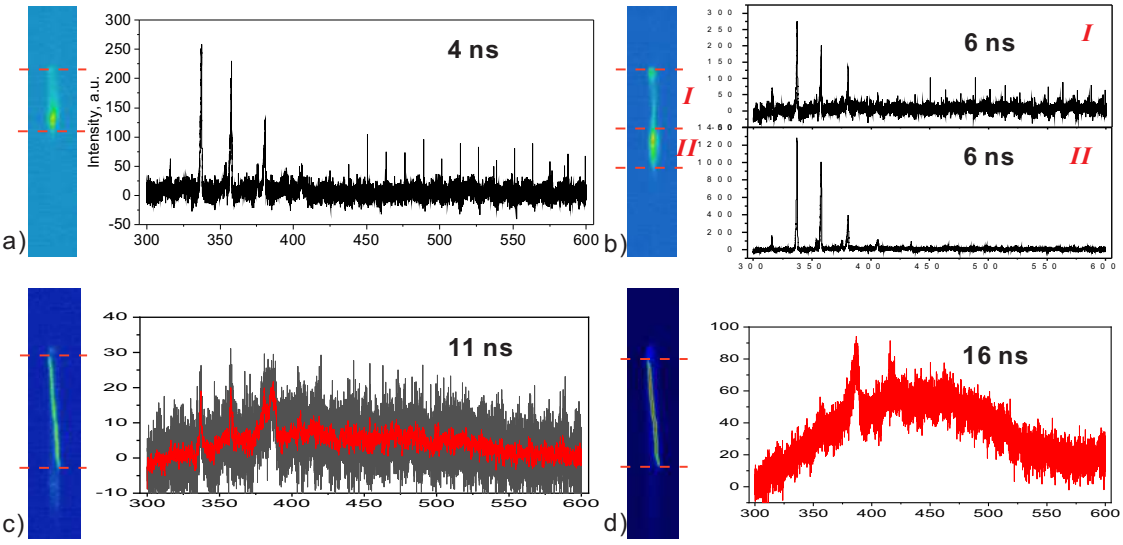

Figure 8. ICCD micro–images from zero order of spectrometer at time instants (a) $t = 4$ ns, (b) $t = 6$ ns, (c) $t = 11$ ns, (d) $t = 16$ ns, as well as spectra of a single discharge channel in the wavelength range of 300–600 nm. Resolution of the optical system is 7.6 μm/pxl. $U = -25$ kV, 6 bar, N_2, ICCD camera gate= 1 ns, 200 accumulations. The spectra are corrected for system spectral sensitivity.

At $t = 2 - 4$ ns, the width of plasma is limited by the opening of the slit. Then,

the discharge channel constricts, but because the time of constriction or of propagation of the channel is smaller than the minimum available gate of the ICCD camera, 0.5 ns, we are not able to register the process. At $t = 6$ ns, the diameter of the plasma channel is much smaller than the initial one and a feather–like structure is observed at the front of the propagating plasma channel. At $t = 8 - 10$ ns, the filament is almost formed but diffuse plasma is still observed near the high-voltage electrode. A typical length of the diffuse region is $0.5 - 0.7$ mm. Finally, at $t = 8 - 10$ ns, the filament "touches" the high–voltage electrode. We intentionally used the same geometry, first for ICCD imaging through the slit of the spectrometer, and then for taking spectra, keeping the entrance slit as narrow as possible at the condition that the filament is not cut by the slit. To get a spectrum, we had to collect ~ 1000 accumulations. Four specific moments (t =4, 6, 11 and 16 ns) were selected for comparing the changes in spectral composition during the streamer–to–filament transition.

An integrated ICCD image taken at zero order of diffraction grating is displayed on the left side of each figure. The spectrum corresponding to this image in the wavelength range of 300–600 nm is shown on the right side of each figure. The spectra are corrected for the spectral sensitivity of the system.

As indicated above and shown in the ICCD image, the discharge at $t = 4$ ns is a "classical" surface streamer nanosecond dielectric barrier discharge (nSDBD) [20]. The image is restricted by the opening of the slit. The spectrum contains second positive system of nitrogen (SPS N_2: $C^3\Pi_u \rightarrow B^3\Pi_g$) with the highest peak at a wavelength of λ =337 nm. The spectrum in the wavelength range over 450 nm does not give any information but shows the electrical and optical noise.

The next frame shows the ICCD image and the spectrum for the time instant $t = 6$ ns. The change in the morphology of the plasma channel is clearly visible: the streamer separates into two regions: a thin channel sometimes not reaching the electrode, marked as region *I* (a bright spot is quite often observed on the electrode edge, a thin channel can reach or not this spot), and a feather–like structure on the front of the plasma channel, or region *II*. The spectra for regions *I* and *II* are similar in composition but different in intensity. Due to almost 5 times higher emission intensity in the region *II*, we can identify more bands of the second positive system.

At time $t = 11$ ns, the channel of the filamentary plasma and the near–electrode plasma have just been connected via a discharge channel with the same diameter as a filament. The diameter is already constant over the length of the discharge channel. Three components are distinguishable in the spectrum, albeit noisy: the second positive system of nitrogen, CN molecular emission of violet system and the continuous wavelength (*cw*) spectrum. The SPS of nitrogen is a "footprint" of a streamer discharge. Three molecular bands of $C^3\Pi_u \rightarrow B^3\Pi_g, 0-0, 0-1$ and $0-2$ still can be seen from the spectrum.

Note that CN molecular band of a violet system is present in the spectra of the filaments of the negative polarity discharge [20]. Some amount of carbon atoms can appear because of non–ideal pumping and partial ablation of the surface of the

dielectric. CN violet system is known to be observed under re–entry conditions, non-directly indicating to a possible high temperature.

At $t = 16$ ns, a well–developed filament with a constant diameter along the channel is already formed. The spectrum contains continuous wave (cw) emission and the CN molecular band of the violet system. The second positive system of nitrogen is no longer observed. This can be due to two reasons: (a) sharp decrease of E/N and so not enough energy to excite $N_2(C^3\Pi_u)$ state; (b) complete dissociation of N_2; and this can be a combination of considered cases (a) and (b).

Similar experiments were carried out at positive polarity, $U = 25$ kV in 6 bar nitrogen. Second positive system of nitrogen can be seen clearly at the streamer phase and at the transition period. The feather–like structure at the front of the filament channel, with less emission intensity compared to the negative polarity discharge, also mainly contains the SPS of N_2. In the well–developed filament channel, the continuous wave spectrum at positive polarity is less intense than the spectrum at negative polarity, which is in agreement with the previous work [21]. Qualitatively, spectral behavior of the streamer–to–filament transition in 6 bar N_2 is very similar for both polarities of the high–voltage pulse.

3.2. Morphology of streamer–to–filament transition at the micro-scale. Diameter of filaments and $x - t$ diagrams

One of the reasons to select the voltage just above the transition threshold and a relatively low pressure was that the transition at these initial parameters happens relatively slowly, in a few nanoseconds instead of 1 ns or less. This allowed detailed analysis of plasma transformation in the process of transition. ICCD imaging was done for the region containing at least a few filaments to see how general the transformations during the transition are.

The micro–scale images of filamentary discharge at $U = \pm 25$ kV in N_2 at 6 bar at six different time instants in the interval $2 - 11$ ns are presented in Figure 9. From the first image, $t = 2$ ns, we can see the propagation of streamer discharges starting from the edge of the high–voltage (HV) electrode. The electrode is indicated as the yellow dash arc in the image. The streamer propagation is shown with the grey dash arc.

At negative polarity, at time instant $t = 5$ ns, channel contraction and formation of a feather–like structure are observed for a few randomly positioned streamers. The intensity of emission of newly formed plasma channels is high compared to surrounding streamers, a few tens of times higher. Not all of them will survive. The "survivors" will form regular a structure of equidistant channels known as filaments ($t = 9$ ns, $t = 11$ ns). The pink dash arc in each frame indicates the tip of a feather–like structure. This structure, appearing at $t = 5$ ns, propagates further, and at $7 - 8$ ns the emission propagating backward along the channel to the direction of the high–voltage electrode is seen. We will call this"backward wave of emission". In Figure 9, the blue dash arcs on the images for $t = 5, 7, 8, 9$ and 11 ns show the propagation of backward wave of

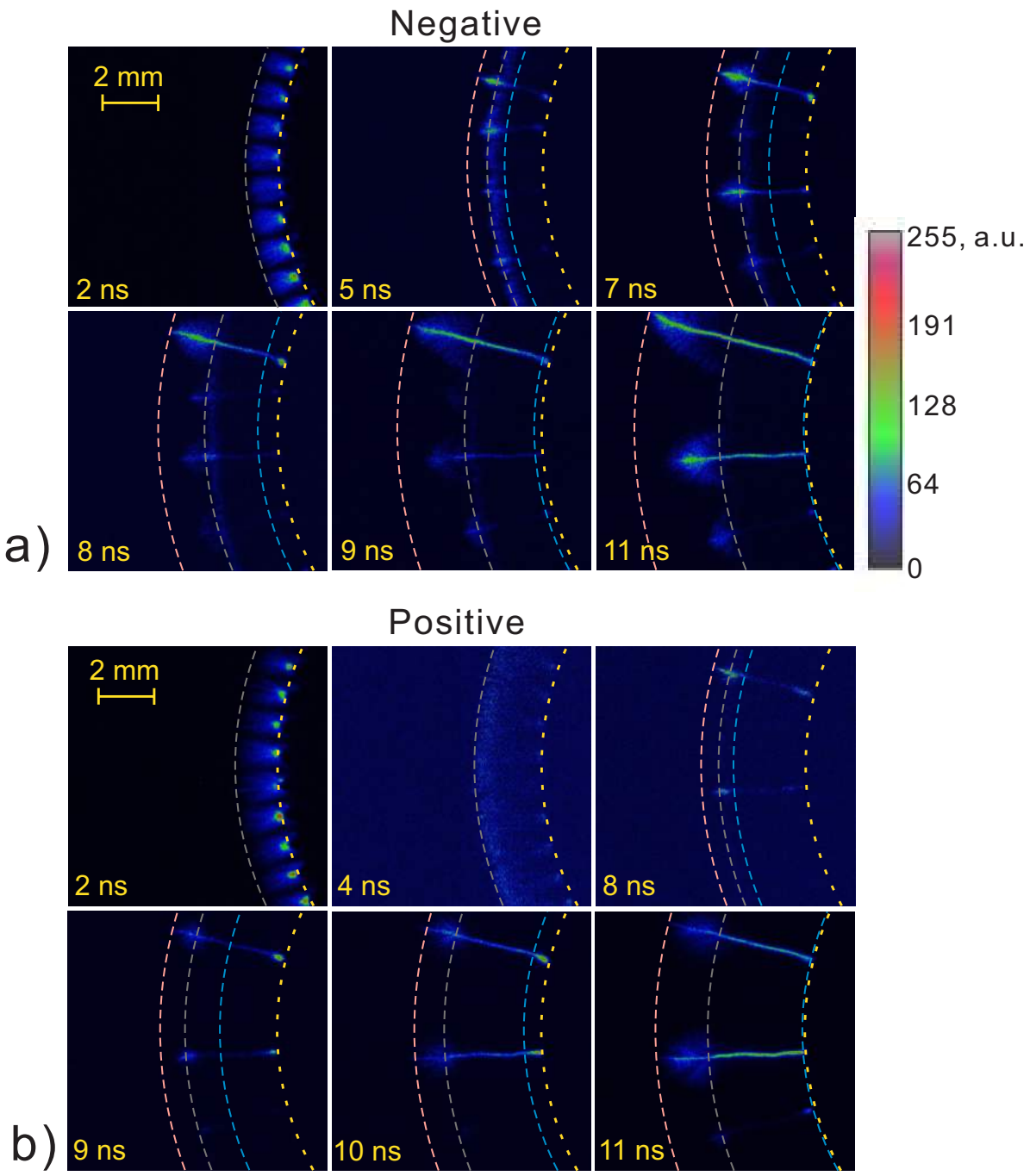

Figure 9. Measure of the position of the streamer front (grey dash), forward emission from the feather–like structure (pink dash), and backward emission (blue dash) from ICCD images of discharge in N_2 at (a) $U = -25$ kV at 6 bar at time instants $t = 2, 5, 7, 8, 9$ and 11 ns; (b) $U = +25$ kV at 6 bar at time instants $t = 2, 4, 8, 9, 10$ and 11 ns. Camera gate is 1 ns. Resolution of the optical system is 7.6 μm/pxl. The yellow dash arc indicates the edge of the HV electrode.Here and further on ICCD images, the false color scheme is so that blue corresponds to minimum intensity (black corresponds to zero intensity), and red corresponds to maximum intensity.

emission. We can see the backward emission propagates as time goes from $t = 5$ to $t = 11$ ns. At $t = 11$ ns, the backward wave of emission almost reaches the edge of the HV electrode.

The picture of the streamer–to–filament transition at positive polarity is similar, with the difference that the emission intensity of streamers sharply drops during their propagation, in the time interval $4 - 8$ ns. The feather–like structure develops from a dark region about 2 mm away from the HV electrode. The backward wave of emission, starting at $t = 8$ ns, propagates towards the HV electrode. Similar to negative polarity, at $t = 11$ ns, the backward wave of emission at positive polarity almost reaches the edge of the HV electrode.

The diameter of discharge channels, "full width at half maximum" (FWHM) of emission intensity, is an essential parameter for analyzing the plasma properties. Two sets of experiments were done at $U = \pm 25$ kV, 6 bar and $U = \pm 35$ kV, 7 bar in nitrogen. They were intended for explaining how the experimental conditions (pressure, amplitude and polarity of applied voltage) influence the diameter of discharge channels. Each ICCD image was obtained by 50 accumulations to increase the signal–to–noise ratio. An open–source software "Fiji" [35] was used for quantitative analysis of the ICCD micro–images, including the measurement of plasma channel diameter. An example of intensity of optical emission across the channel and corresponding ICCD image for a selected point are shown in Fig. 10b. The level of noise as well as the emission profile structure are clearly seen from the figure.

To evaluate the effect of the amplitude of applied voltage and of the number of accumulations on the measured diameter of the discharge channels, two additional sets of experiments with different number of accumulations were done by varying the amplitude of the applied voltage. As shown in Figure 10, the diameter of a plasma channel in a single–shot mode is almost 2.5 times smaller than the diameter calculated from the images accumulated for 50 times. It can be seen from the figure that the diameter of discharge channels practically does not depend on the amplitude of the applied voltage. We consider measurements in a single–shot regime as a physical limit for the measurements of the diameter: the error at higher number of accumulations is possible because of slightly different development of a plasma channel from pulse to pulse. Knowing that the maximum possible error at 50 times averaging is almost a factor of 2, we nevertheless will continue measurements with 50 accumulations with a camera gate of 1 ns to get at least qualitative information about the temporal dynamics of the transition.

Full width at half maximum (FWHM) of emission intensity of plasma channels observed by ICCD camera as a function of time at 50 accumulations is plotted in figure 11 (a) for $U = -25$ kV, 6 bar discharge in nitrogen. The data are presented for different distances d from the high–voltage electrode taken as a parameter. The distance d changed in the range of 160 μm $-$ 4 mm.

It is interesting to note that in spite of the observed constriction of the channel, the spectrum of the discharge before $9 - 10$ ns corresponds to the optical spectrum of

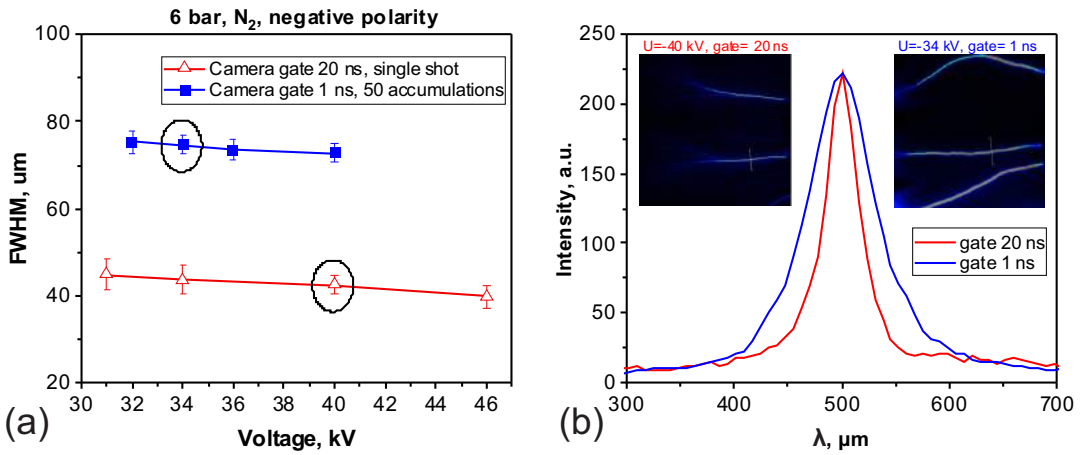

Figure 10. (a) Full width at half maximum (FWHM) of discharge channels for different amplitudes of the applied voltage and different number of accumulations and (b) normalized intensity of two selected points: gate 1 ns, U=-34 kV (blue curve) and gate 20 ns, U=-40 kV (red curve). Negative polarity, 6 bar, nitrogen.

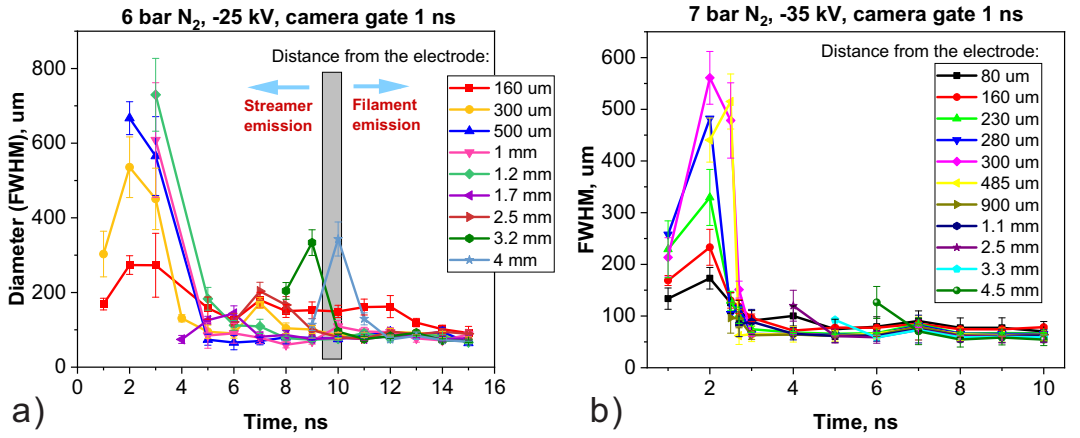

Figure 11. The diameter of discharge channel as the full width at half maximum (FWHM) of discharge optical emission at different positions from the HV electrode in N_2: (a) $U = -25$ kV, 6 bar; (b) $U = -35$ kV, 7 bar.

a streamer with the dominant second positive system of molecular nitrogen. The grey vertical rectangle in figure 11 (a) designates a region where the emission changes to the *cw* spectrum typical for the filaments.

Figure 11 (b) shows the FWHM of emission of plasma channels at $U = -35$ kV, 6 bar in N_2 at different positions from the HV electrode. Note that the emission intensity profiles used to calculate the diameter are less noisy at $U = -35$ kV than at $U = -25$ kV due to the higher emission intensity at higher voltage. At distances less than 500 μm from the electrode, all the curves demonstrate the same trend: the diameters of the plasma channels increase due to the expansion of streamers and then abruptly shrink

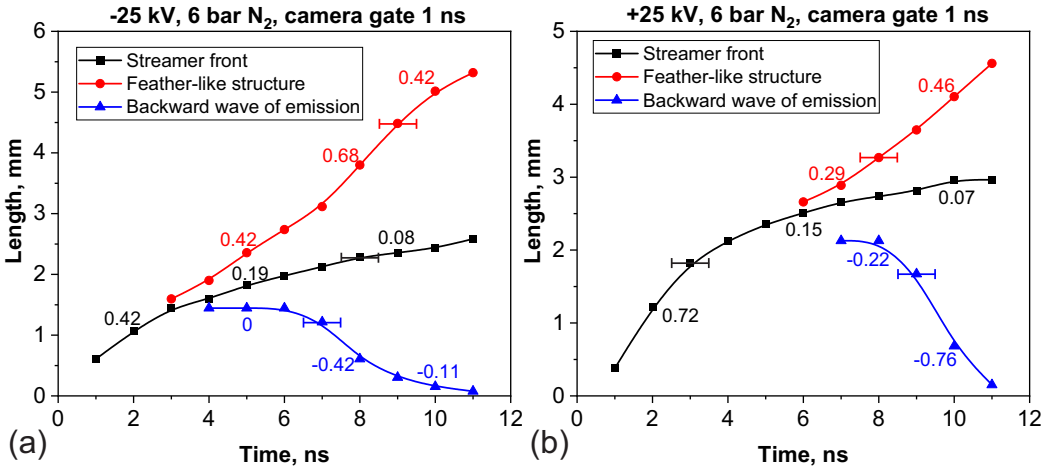

Figure 12. The $x-t$ diagrams of streamer front, feather–like structure and backward wave of emission at (a) $U = -25$ kV and (b) $U = +25$ kV. Nitrogen, 6 bar. The propagation velocity is marked in the plots as numbers in unit of mm/ns.

to less than 100 μm at $t = 2-3$ ns. At times after $t = 4$ ns, nearly everywhere along the plasma channel, the diameter is less than 100 μm. This is a "footprint" of a start of a streamer–to–filament transition.

Note that streamers and filaments are not necessarily objects of a cylindrical shape. A specially designed electrode with a discharge developing on the lateral surface of the cylinder allowed to study streamers and filaments from a side view. Although measurements were done only at atmospheric pressure $U = +20$ kV nSDBD in air, it was found that the streamers have the dimensions of 620 μm $\times$ 270 μm; the shape is flattened in a direction perpendicular to the dielectric surface. There is therefore no reason to think that the discharge channel is cylindrical in other experimental conditions.

Finally, figure 12 presents $x-t$ diagrams obtained from the ICCD images shown in the figure 9. The propagation length of a streamer front (black curve), feather–like structure (red curve) and backward wave of emission (blue curve) are plotted for both negative and positive polarities. The absolute values of propagation velocities for streamers, feather–like structures and backward emission are presented near the plots in mm/ns units. It can be seen that, for the same experimental conditions ($U = \pm 25$ kV, 6 bar nitrogen), the negative polarity feather–like structure (red curve) propagates faster than the positive one, while the backward wave of emission propagates much slower at negative polarity. The positive polarity streamer propagates faster at the beginning, and later, during the extinction, it has almost the same velocity as the negative polarity streamer. At the same time $t = 11$ ns, streamers at both polarities stop to propagate when the backward wave of emission reaches the HV electrode. At the same time the *cw* spectrum appears in optical emission. It can also be seen from the $x-t$ diagrams that the separation of a feather–like structure and backward wave of emission appears earlier at negative polarity ($t = 3-4$ ns) than at positive polarity ($t = 6-7$ ns).

3.3. Analysis of the "point of origin" of the filament

The present paper is limited to observations in the direction perpendicular to the surface of the dielectric, but even with this limitation, we can ask the question, at what distance from the electrode is the beginning of the filament, the point at which the transition occurs.

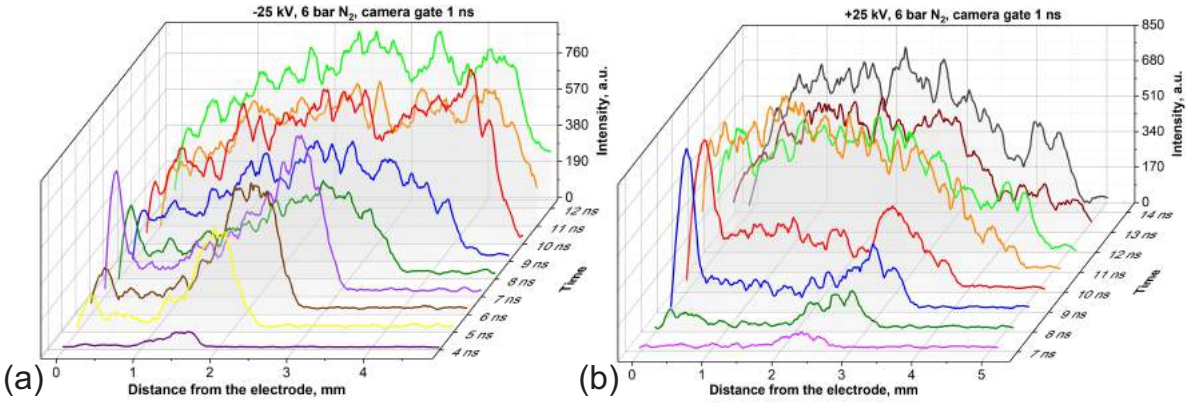

Figure 13. 3D diagram of emission intensity distribution along discharge channel at (a) $U = -25$ kV from time $t = 4$ to 12 ns and (b) $U = +25$ kV at time $t = 7$ and 14 ns in N_2 at 6 bar. The same colors mean the same time delay from the beginning of the discharge emission.

A complex structure of the contracted channel is confirmed by the 3D diagrams of the emission intensity distribution along the discharge channel taken at $U = \pm 25$ kV in N_2 at 6 bar with the camera gate 1 ns (figure 13). Four time moments were selected differently for negative and positive polarity of discharge according to their different propagation behavior. The color bars in the figure have been unified for both polarities in order to make a better comparison. From figure 13 (a), we can see that at negative polarity the contracted channel appears at $t = 4$ ns. At $t = 5$ ns, there is a spot with a high emission intensity near the HV electrode. Starting from this moment, there are two maxima of the emission intensity: one region is close to the HV electrode and the other one is a feather–like structure always observed at the front of the contracted channel. For $t = 5$ to 7 ns, we can clearly see the increase of emission intensity of the feather–like structure and propagation of the emission further from the HV electrode. At the same time, we observe propagation of a wave of emission from the same point back to the high–voltage electrode.

If we consider a fixed point, e.g. 0.8 mm from the HV electrode, the emission intensity increases in the period $\Delta t = 4 - 7$ ns due to the passage of the back wave. When the backward wave of emission approaches the HV electrode ($t = 9$ ns), the bright spot near the electrode decays. No two separate emission zones are observed any more. Starting from $t = 9$ ns, the emission intensity along the whole discharge channel increases as the discharge propagates; it is exactly the moment when the streamer–like

spectra change to the (cw) and atomic lines spectra.

For a positive polarity discharge with the same amplitude of the applied voltage, figure 13 (b) shows similar trends as for a negative polarity one. The emission intensity of the spot near the electrode is even higher than the intensity of the feather–like structure. There is a jump between $t = 10$ and 11 ns which is exactly the moment when the backward wave of emission propagates until the HV electrode. Starting from $t = 11$ ns, the intensity along the whole discharge channel increases sharply to a high value and stays the same as the discharge propagates.

Three parameters were monitored in time and in space with the aim of finding the origin of the filament: the FWHM, the amplitude of H_α line of atomic hydrogen ($\lambda = 656.3$ nm), and the amplitude of CN emission. To study H_α emission, 5% of H_2 was added to nitrogen. The total pressure was kept constant and equal to 5 bar.

Preliminary analysis of time–resolved H_α spectra integrated on the whole discharge region demonstrated that at $t = 5$ and 6 ns, no H_α emission is observed; the SPS of molecular nitrogen dominates in the spectra. Starting from $t = 7$ ns, the H_α peak appears and the intensity of emission increases progressively. At $t = 9$ ns, the H_α peak is well defined and the second order of SPS system of nitrogen disappears. Combining this information with the discharge images shown in figure 7, one can find that the time interval $\Delta t = 7 - 10$ ns is the interval where the backward wave of emission propagates from the feather–like structure to the high–voltage electrode.

The spectra of the discharge taken for the interval $\lambda = 635{-}675$ nm with time delays from $t = 7$ to 10 ns were analysed for different distances d from the HV electrode. The spatially–resolved spectra accompanied by the micro–images of the discharge channel at $t = 7 - 10$ ns are presented in figure 14 (a). The HV electrode is on the top of each image and the discharge propagates downwards to the ground electrode on the bottom. Each image is divided into 5 regions, marked as region I, II, III, IV and V. From top to bottom, the distance from the HV electrode d is equal to $0 - 0.8$ mm, $0.8 - 1.6$ mm, $1.6 - 2.4$ mm, $2.4 - 3.2$ mm and $3.2 - 4$ mm.

The very first sign of H_α emission appears at $t = 7$ ns in the region II, $d = 0.8 - 1.6$ mm from the electrode. At $t = 8$ ns, the H_α peaks spread in both directions, appearing in region II, III and IV. At $t = 9$ ns, the H_α line emission is observed in the whole region. At $t = 10$ ns, the H_α line increases in intensity, designating a well–developed filament.

The electron density was calculated from the FWHM of H_α emission as described in [21]. The normalized H_α line emission at $t = 8, 9$ and 10 ns at different distances from the HV electrode are shown in figure 14 (b). The electron density is the same for all the distances and exhibits a small decay from $t = 8$ ns to $t = 10$ ns. High, almost constant electron density, $(1 - 2) \cdot 10^{19}$ cm^{-3}, observed in the region near the electrode ($0 < d < 4$ mm) in the present work, is in excellent agreement with the electron densities measured before and integrated over the filament, up to 10 mm in length [20, 21].

The amplitude of H_α line, assuming that quenching is identical along the plasma channel, indicates relative density of excited hydrogen atoms. CN emission, as described

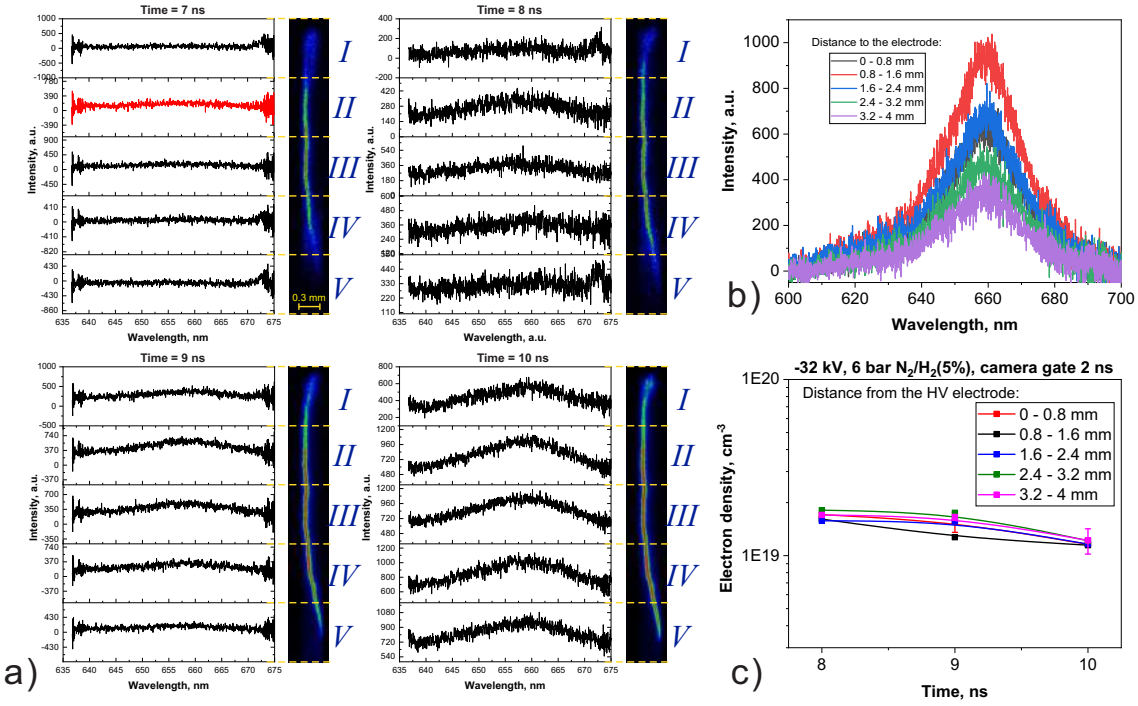

Figure 14. (a) Spatially resolved H_α lines from $t = 7$ to $t = 10$ ns, (b) spatially resolved H_α intensity at different positions from the HV electrode at $t = 10$ ns and (c) spatially resolved electron density measured from H_α lines at $t = 8$, 9 and 10 ns in the process of streamer–to–filament transition. $U = -32$ kV, 6 bar, N_2/H_2 (5%), ICCD camera gate 2 ns and 1000 accumulations per frame.

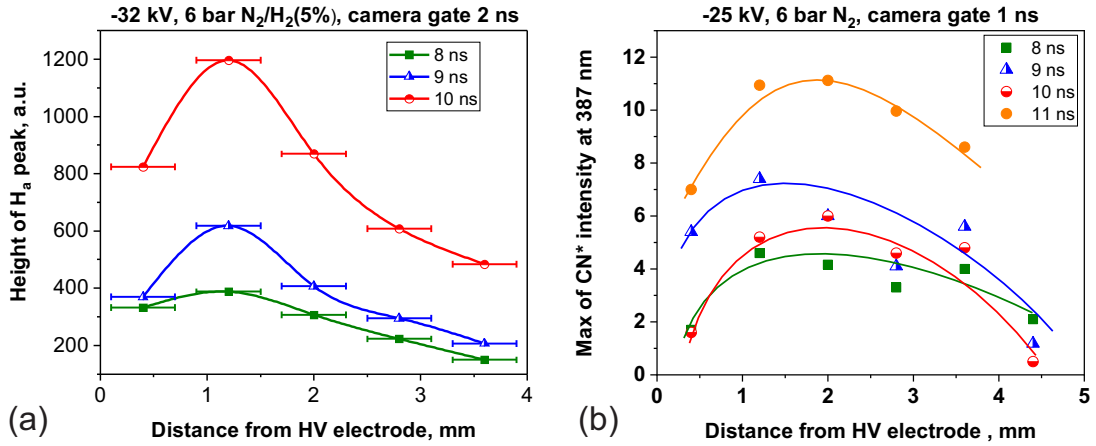

Figure 15. Maximum intensity of (a) H_α lines from $t = 8$ to $t = 10$ ns and (b) CN bands at 387 nm from $t = 8$ to $t = 11$ ns in the process of streamer–to–filament transition.

above, is in strong correlation with the *cw* spectrum but easier to trace and indicates relative intensity of *cw* emission. Peak emission intensities for H_α and CN emission as a function of distance from the high–voltage electrode for the time interval $\Delta t = 8 - 10$ ns

is presented in figure 15 (a) and figure 15 (b) respectively. As time goes from $t = 8$ to $t = 11$ ns, the emission intensity of both H_α line and CN band increases. The highest emission intensity of H_α line appears in the region II, $0.8 - 1.6$ mm from the HV electrode, while the CN band has the maximum intensity in the region III, at the position 2 mm from the HV electrode. It is important to note that we observe the origin of H_α and CN emission (and so, a start point of streamer–to–filament transition) at a significant $1 - 2$ mm distance from the HV electrode. The first stage of transition is the shrinking of a streamer channel and so, increase of the current density. The second stage is the propagation of a feather–like structure from the high–voltage electrode and of a back wave to the high–voltage electrode.

4. Discussion

A new phenomenon observed in a single–shot high–pressure nSDBD is the appearance, on a front of merged surface streamers, of a plasma zone moving with a higher velocity (see figure 9). A bi–directional ionization wave, one wave moving forward and another backward to the high–voltage electrode, is recorded in the experiment as two waves of optical emission described above. One wave, a feather–like structure, propagates in the direction away from the HV electrode (red curve in figure 12), charging the dielectric surface *via* a system of surface streamers. Another wave, a backward wave of emission, propagates towards the HV electrode (blue curve in figure 12) along an already charged surface of a thin channel, so a streamer "shell" as a precursor of the propagating wave is not needed. These two waves start from a small (microscopic) region also moving forward from the high–voltage electrode.

Formally, this phenomenon is similar to the space stem in lightning, an elongated plasma zone which forms at the border of the streamer zone of the negative leader, initiates the formation of positive and negative streamers and determines the stepwise mechanism of negative leader propagation [36–39]. For this reason we suggest to call this starting point of the two oppositely directed waves, or presumably a microscopic elongated plasma region, a "surface stem". There is still insufficient data to claim the identity of the mechanism of space stem and surface stem formation. In particular, the surface stem is formed over nanoseconds, while the space stem [36]— over tens of microseconds. One of the key questions is how the surface stem is formed in nSDBD. At the moment, this question seems to be the most important in understanding of the filamentation mechanism.

One of the possible reasons for the formation of a surface stem is the development of the instability of the plane front of the ionization wave, or Laplace instability [40–43]. This is an instability of the discharge front to bending disturbances with a characteristic size greater than or of the order of the front thickness [41, 42]. The physical nature of this instability is associated with a local enhancement of the field, in the region of future surface stems at the front of the ionization wave. This leads to an increase in the rate of elongation of these zones and an increase in their electron density, which further

enhances the field.

At the initial stage of evolution (see figures 4, 5 and 9), all nSDBD streamers start synchronously from the edge of the high–voltage electrode. The diameters of the streamers increase with the distance from the electrode, and simultaneously propagating streamers merge into a single front. Starting from this point, the propagation of streamers can be considered as the propagation of an ionization wave with an almost uniform front or as a wave of surface charging. This is true both for the streamers starting from the smooth edge of the disk–shaped high–voltage electrode and for the streamers starting from the teeth of the gear–shaped electrode: at a sub–millimeter scale at 6 bar, the front at $3-4$ ns is already uniform (figures 4–5). As a result, the field in the head of each streamer in the front is screened by the neighbors and becomes smaller than the field in the head of a single streamer. Significant and sharp increase of the electric field and the electron density occurs in the parts of the ionization front where the instability develops. In the zone of the enhanced field, new–born surface streamers charge the dielectric surface in front of the propagating discharge channel. This may explain the shape of a feather–like structure (see figures 4, 9 at $t = 7-8$ ns for negative polarity and figures 5, 9 at $t = 8-9$ ns for positive polarity). Will remind that at this time period we do not see yet the atomic lines in the spectrum and so the electron density anywhere in space is still much lower than the electron density in the filaments a few nanoseconds later.

Transverse dimensions of a surface stem are significantly smaller than the diameter of the streamer at the point where the surface stem appears. Will suppose that the diameter of a surface stem is close to the diameter of a thin channel connecting the electrode and the feather-like structure. According to figure 11, the diameter of a thin channel is at least 10 times smaller than the diameter of the streamer. As a consequence, one should expect a 100–fold increase in the current density in the surface stem and, accordingly, approximately the same increase in the electron density.

As a result of such a "collapse" of the channel and increase in the ionization degree, there should be a significant redistribution of the potential near the poles of the surface stem and a formation of positive and negative ionization waves (or a bi–directional ionization wave). These ionization waves propagate in the form of potential gradient waves without noticeable attenuation under the condition that the ionization degree in the channels ahead of the front of these waves N_e/N is low. In nitrogen (no attachment) the decay of electron density will be determined by the rate of electron–ion recombination; at $P = 6$ atm, the main positive ion will be N_4^+ with a recombination coefficient $\beta = 2{\cdot}10^{-6}{\cdot}(300/T_e)^{0.5}$ cm^3/s [44]. In the field range $E/N = 60-100$ Td, the electron temperature is approximately $T_e = 1.5-2$ eV, therefore $\beta = 2.4 \cdot 10^{-7}$ cm^3/s. In this case, $\tau \cdot N_e = \beta^{-1} \approx 4 \cdot 10^6$ cm^{-3}·s, that is, at $\tau = 2$ ns, the electron density is equal to $N_e \approx 2 \cdot 10^{15}$ cm^{-3}. Will note that the obtained value is close to the typical electron density in surface streamers: it comprises $N_e \approx 10^{15}$ cm^{-3} at atmospheric pressure [45–47] and $N_e \approx 10^{16}$ cm^{-3} at pressure of 6 bar [31].

To ensure the propagation of a fast ionization wave (FIW), it is necessary [48]

that the time of formation of the next element of plasma channel after the front of the ionization wave, $\tau_{FIW} = R/v_{FIW}$, be much shorter than the time of polarization of a weakly ionized gas ahead of the FIW front (here R is the radius of the channel, v_{FIW} is the speed of the FIW). Otherwise, a rapid blurring of the front and stopping of the ionization wave will be observed.

The polarization time of the channel with length L and radius R is

$$\tau_{pol} = \frac{1}{4\pi\sigma} \cdot \frac{(L/2R)^2}{ln\,(L/R)} \tag{1}$$

where σ is the channel conductivity. In the case where electron–neutral collisions dominate over electron–ion collisions, $\sigma \sim N_e/N$. At $P = 6$ atm, $L = 2$ mm, $R = 50$ μm (see figure 11) and an electron density in the channel of $N_e = 2 \cdot 10^{15}$ cm^{-3}, we obtain a polarization time for such a channel of $\tau_{pol} \approx 0.4$ ns. Therefore, in order for the front of the potential gradient wave not to "blur" when it moves along the track of streamer channels, the velocity of this wave should be $v_{FIW} \gg 10^7$ cm/s, which is consistent with the experimental data, where the recorded velocities are $(2-7) \cdot 10^7$ cm/s (figure 12).

When the backward wave of emission reaches a zone close to the high–voltage electrode, a high current flows through the thin channels, and the fast gas heating [23] provides a transition to the LTE state with high electron density: the filaments are formed.

A similar phenomenon, namely the formation of a bi–directional ionization wave, was observed in the recently published work [49], which presents the dynamics of ionization waves in a sinusoidally driven high–voltage (15.43 kHz, 25 kV$_{pp}$ peak–to–peak) surface barrier discharge in atmospheric–pressure air. The authors observed, using sub–nanosecond–resolved optical emission spectroscopy based on the time–correlated single–photon counting (TCSPC) technique, a remote streamer initiation on dielectric surface. In the negative half–period, a bi–directional ionization wave formed at the border of the streamer zone, similar to surface stems and bi–directional ionization waves in the present work. The velocities of the ionization waves in [49] were equal to $(1–2) \cdot 10^7$ cm/s. Upon reaching the HV electrode, the cathode–directed ionization wave formed a cathode spot of increased intensity, which, in turn, initiated formation of a highly conductive plasma channel.

An important distinguishing feature of [49] compared to the present work is that it was carried out in a repetitively pulsed SDBD, where an important role should be played by the charge remaining on the dielectric after previous pulses (see review [12]). This complicates the analysis of the results [49]. In addition, in [49] all the main processes occur at microsecond times, that is, at times longer than gas–dynamic rarefaction of channels (for a typical radius of the channel $R \leq 300$ μm). As a consequence, gas heating in the discharge channel should be accompanied by a drop in the particle density, an increase in E/N, and the development of ionization–heating instability [50]. Under the conditions of this work, the characteristic times of the main processes do not exceed 1–2 ns, that is much shorter than the characteristic gas–dynamic times for the region

where the surface stem is formed. That is, ionization–heating instability in this region can not explain the origin of the streamer–to–filament transition.

Therefore, the ionization wave propagating towards the HV electrode should reach the edge of the electrode and form a cathode (or anode) spot there. The spots provide a high current flowing through the channel, finalizing a transition from streamer to filament. In the case of discharges of negative polarity, the filamentation mechanism can be due to the field emission [23, 51]. In the case of positive polarity, the filamentation mechanism in the framework of the suggested model is not yet fully understood. In the process of filamentation, the fast gas heating provides, during nanoseconds or even part of a nanosecond, transition to a state close to LTE, with almost complete dissociation of molecules and a very high ionization degree. Reactions of dissociation of nitrogen molecules via electronically excited states of N_2 lead to a rapid increase in the dissociation degree. This results in a significant increase in the fraction of atomic N^+ ions, which quickly become the dominant type of ions. The coefficients of electron–ion recombination of atomic ions are significantly lower than those of molecular ions [52]. The slowing down of recombination leads to a significant increase in the ionization degree.

From the above, we can conclude that the development of an instability of the plane front of the ionization wave (Laplace instability) and further formation of a surface stem providing a bi–directional ionization wave can be a key element of the filamentation mechanism. It is on the study of this phenomenon that one should, apparently, focus in order to confirm (or refute) this statement.

It should also be noted that studies of processes between a streamer channel and a dielectric play an important role. In a very recent work [53], it was shown that streamer–to–filament transition may occur in a very thin layer between the streamer itself and the electron–depleted zone near the dielectric surface. This is possible under conditions of enhanced ionization in this thin layer, including stepwise ionization [54] from high–energy electronically excited states, starting from $N_2(C^3\Pi_u)$. In [53], a theory of stepwise ionization of hydrogen–like atoms is transferred to molecular nitrogen. The model explains dependence of streamer–to–filament transition in N_2:O_2 mixtures on oxygen admixtures for the pressure range $2-10$ atm and voltage amplitudes $25-55$ kV, and is in good agreement with the experiments [21]. Quenching of excited $N_2(C^3\Pi_u)$ molecules by O_2 leads to a decrease in the ionization frequency and, accordingly, to an increase in the voltage at which a streamer–to–filament transition occurs. However, it should be noted that the model [53] demands an enhanced flux of ionization from highly electronically excited states of N_2 — accordingly, it is assumed [53] that the ionization frequency of $N_2(C^3\Pi_u)$ should exceed the frequencies of dissociation and quenching of this state by electron impact. According to TALIF measurements of N–atom density and corresponding kinetic calculations [55], at a specific delivered energy of about a few eV per particle, and electric fields in the mentioned range, $E/N = 150 - 300$ Td, the electron collisions with $N_2(A^3\Sigma_u^+, B^3\Pi_g, C^3\Pi_u)$ states result mainly in dissociation of these states. Mentioned contradiction means that the question of the role of stepwise

ionization of $N_2(C^3\Pi_u)$ in the thin layer between the streamer and the dielectric surface requires additional experimental (although complicated as far as sub–micron resolution and a side view on the streamer are needed) and theoretical studies.

5. Conclusions

The fine structure of a streamer–to–filament transition in a single–shot high–voltage nanosecond surface dielectric barrier discharge (nSDBD) in molecular nitrogen at a pressure of $P = 6$ bar was studied with the help of ICCD microimaging.

It was shown that, for both polarities of the high–voltage electrode, there is an intermediate discharge structure appearing a few nanoseconds before the transition and leading to the transition.

When propagating in radial direction from the high–voltage electrode, the surface streamers slow down during the 2-4 first nanoseconds. A formation of thin channels, tens of microns in diameter, is observed inside some of them. The diameter of the considered channels is at least an order of magnitude smaller than the typical diameter of a surface streamer at this point, $200 - 600$ μm.

A few nanoseconds later, a feather–like structure accumulating surface micro–streamers, is observed at the front of each thin channel. The feather–like structure propagates forward, from the high–voltage electrode. A backward wave of emission starts from the same point and propagates towards the edge of the high–voltage electrode.

The optical emission from a single thin channel is the same in spectral composition than the emission from the streamer. The emission from the feather–like structure is a few times higher in intensity compared to the intensities of emission from the streamer and from the thin channel. During this transition period, which lasts 4-6 nanoseconds, the diameter of the surface stem channel stays small (tens of μm), resulting in a significant increase in specific delivered energy.

High electron density, $n_e \sim 10^{19}$ cm^{-3}, and the continuous wavelength (cw) emission appear along the channel 1-2 ns before the backward wave of emission reaches the edge of the high–voltage electrode. A time resolution of 1 ns is not sufficient to see a point of origin and/or propagation of high electron density and (cw) emission. From this, we conclude that the speed of a new–born filament, when traveling along the surface, should be close to the speed of the FIWs in moderate pressure systems, that is centimeters per nanosecond. In the external zone not "pre–treated" by streamers, the speed of propagation of filaments is limited by the appearance of micro–streamers near the head of the propagating filament and it is lower. Finally, the maximum of H_α emission (and so the maximum density of excited atoms) is situated at a distance of $1 - 1.5$ mm from the edge of the electrode.

Provided theoretical analysis suggests that streamer–to–filament transition can start as a result of the instability of the plane front of the ionization wave, or Laplace instability. The physical nature of this instability is associated with a local enhancement

of the field at the front of the ionization wave created by merged streamers. As a result, a surface stem should be formed, a specific region with enhanced electron density too small to be observed experimentally under conditions of the present work. The experimental sign of formation of a surface stem is the appearance, from the same point, of two oppositely–directed ionization waves, observed as a feather–like structure and a backward emission. These ionization waves propagate in the form of waves of a gradient of potential without noticeable attenuation under the condition that the ionization degree in the channels ahead of the front of these waves is low.

When the backward wave of emission reaches a zone close to the high–voltage electrode, a high current flows through the thin channels, and the fast gas heating provides a transition to the LTE state with high electron density: the filaments are formed.

Acknowledgements

The work was partially supported by French-Russian international research project IRP "Kinetics and physics of pulsed plasmas and their afterglow" (CNRS financial and organization support), the French National Research Agency (ASPEN Project) and the French General Directorate of Armaments (DGA) under the EP-DGA convention 2790 "Interaction of detonation with low temperature plasma". The support of China Scholarship Council (CSC) for Chenyang Ding is gratefully acknowledged. The authors are thankful to Pascal Pariset and Bruno Dufour for engineering support.

References

[1] Siemens W 1857 Ueber die elektrostatische induction und die verzögerung des stroms in flaschendrähten *Annalen der Physik* **178** 66–122

[2] Andrews T and Tait P G 1860 On the volumetric relations of ozone, and the action of the electrical discharge on oxygen and other gases *philosophical transactions of the royal society* **150** 113–131

[3] Brandenburg R 2017 Dielectric barrier discharges: progress on plasma sources and on the understanding of regimes and single filaments *Plasma Sources Science and Technology* **26** 053001

[4] Tu X and Whitehead J 2012 Plasma-catalytic dry reforming of methane in an atmospheric dielectric barrier discharge: Understanding the synergistic effect at low temperature *Applied Catalysis B: Environmental* **125** 439–448

[5] Chang J 2008 Physics and chemistry of plasma pollution control technology *Plasma Sources Science and Technology* **17** 045004

[6] Brandenburg R, Barankova H, Bardos L, Chmielewski A G, Dors M, Grosch H, Hołub M, Jogi I, Laan M, Mizeraczyk J *et al.* 2011 Plasma-based depollution of exhausts: principles, state of the art and future prospects *Monitoring, control and effects of air pollution* (InTech) pp 229–254

[7] Schmidt M, Jõgi I, Hołub M and Brandenburg R 2015 Non-thermal plasma based decomposition of volatile organic compounds in industrial exhaust gases *International journal of environmental science and technology* **12** 3745–3754

[8] Tanaka Y 1955 Continuous emission spectra of rare gases in the vacuum ultraviolet region *JOSA* **45** 710–713

[9] Kogelschatz U, Esrom H, Zhang J Y and Boyd I 2000 High-intensity sources of incoherent uv and

vuv excimer radiation for low-temperature materials processing *Applied Surface Science* **168** 29–36

[10] Mariotti D, Belmonte T, Benedikt J, Velusamy T, Jain G and Švrček V 2016 Low-temperature atmospheric pressure plasma processes for "green" third generation photovoltaics *Plasma Processes and Polymers* **13** 70–90

[11] Matthes R, Bender C, Schlüter R, Koban I, Bussiahn R, Reuter S, Lademann J, Weltmann K D and Kramer A 2013 Antimicrobial efficacy of two surface barrier discharges with air plasma against in vitro biofilms *PloS one* **8** e70462

[12] Leonov S B, Adamovich I V and Soloviev V R 2016 Dynamics of near-surface electric discharges and mechanisms of their interaction with the airflow *Plasma Sources Science and Technology* **25** 063001

[13] Samimy M, Webb N and Esfahani A 2019 Reinventing the wheel: Excitation of flow instabilities for active flow control using plasma actuators *Journal of Physics D: Applied Physics* **52** 354002

[14] Starikovskiy A and Aleksandrov N 2021 Gasdynamic flow control by ultrafast local heating in a strongly nonequilibrium pulsed plasma *Plasma Phys Reports* **47** 148–209

[15] Boumehdi M A, Stepanyan S A, Desgroux P, Vanhove G and Starikovskaia S M 2015 Ignition of methane-and n-butane-containing mixtures at high pressures by pulsed nanosecond discharge *Combustion and Flame* **162** 1336–1349

[16] Kosarev I, Khorunzhenko V, Mintoussov E, Sagulenko P, Popov N and Starikovskaia S 2012 A nanosecond surface dielectric barrier discharge at elevated pressures: time-resolved electric field and efficiency of initiation of combustion *Plasma Sources Science and Technology* **21** 045012

[17] Starikovskiy A and Aleksandrov N 2013 Plasma-assisted ignition and combustion *Progress in Energy and Combustion Science* **39** 61–110

[18] Starikovskaia S 2014 Plasma-assisted ignition and combustion: nanosecond discharges and development of kinetic mechanisms *Journal of Physics D: Applied Physics* **47** 353001

[19] Stepanyan S, Starikovskiy A, Popov N and Starikovskaia S 2014 A nanosecond surface dielectric barrier discharge in air at high pressures and different polarities of applied pulses: transition to filamentary mode *Plasma Sources Science and Technology* **23** 045003

[20] Shcherbanev S, Khomenko A Y, Stepanyan S, Popov N and Starikovskaia S 2017 Optical emission spectrum of filamentary nanosecond surface dielectric barrier discharge *Plasma Sources Science and Technology* **26** 02LT01

[21] Ding C, Khomenko A Y, Shcherbanev S and Starikovskaia S 2019 Filamentary nanosecond surface dielectric barrier discharge. experimental comparison of the streamer-to-filament transition for positive and negative polarities *Plasma Sources Science and Technology* **28** 085005

[22] Moralev I V 2017 Private communications *Private communications*

[23] Shcherbanev S, Ding C, Starikovskaia S and Popov N 2019 Filamentary nanosecond surface dielectric barrier discharge. Plasma properties in the filaments *Plasma Sources Science and Technology* Submitted PSST-102956

[24] Stritzke P, Sander I and Raether H 1977 Spatial and temporal spectroscopy of a streamer discharge in nitrogen *Journal of Physics D: Applied Physics* **10** 2285

[25] Albrecht H, Bloss W, Herden W, Maly R, Saggau B and Wagner E 1977 New aspects on spark ignition Tech. rep. SAE Technical Paper

[26] Orrière T, Moreau E and Pai D Z 2018 Ionization and recombination in nanosecond repetitively pulsed microplasmas in air at atmospheric pressure *Journal of Physics D: Applied Physics* **51** 494002

[27] Minesi N, Stepanyan S, Mariotto P, Stancu G and Laux C 2020 Fully ionized nanosecond discharges in air: the thermal spark *Plasma Sources Sci. Technol.* **29** 085003

[28] Shao T, Tarasenko V F, Zhang C, Lomaev M I, Sorokin D A, Yan P, Kozyrev A V and Baksht E K 2012 Spark discharge formation in an inhomogeneous electric field under conditions of runaway electron generation *Journal of Applied Physics* **111** 023304

[29] Lomaev M, Rybka D, Sorokin D, Tarasenko V and Krivonogova K Y 2009 Radiative characteristics

of nitrogen upon excitation by volume discharge initiated by runaway electron beam *Optics and Spectroscopy* **107** 33–40

[30] Orrière T 2018 *Confinement microméetrique de déecharges pulsées nanosecondes dans l'ais a pression atmosphérique et effets électro-aérodynamiques* Ph.D. thesis University of Poitiers France (in French)

[31] Chen X, Zhu Y, Wu Y, Hao J, Ma X and Lu P 2021 Numerical investigations of nanosecond surface streamers at elevated pressure *Plasma Sources Sci. Technol.* **30** 075008

[32] Shcherbanev S A, Popov N A and Starikovskaia S M 2017 Ignition of high pressure lean H_2: air mixtures along the multiple channels of nanosecond surface discharge *Combustion and Flame* **176** 272–284

[33] Anikin N, Starikovskaia S and Starikovskii A Y 2004 Study of the oxidation of alkanes in their mixtures with oxygen and air under the action of a pulsed volume nanosecond discharge *Plasma physics reports* **30** 1028–1042

[34] Anikin N, Starikovskaia S and Starikovskii A Y 2002 Polarity effect of applied pulse voltage on the development of uniform nanosecond gas breakdown *Journal of Physics D: Applied Physics* **35** 2785

[35] Schindelin J, Arganda-Carreras I, Frise E, Kaynig V, Longair M, Pietzsch T, Preibisch S, Rueden C, Saalfeld S, Schmid B *et al.* 2012 Fiji: an open-source platform for biological-image analysis *Nature methods* **9** 676–682

[36] Bazelyan E M and Raizer Y P 2000 *Lightning physics and lightning protection* (Bristol, London, UK: IOP Publishing)

[37] Rakov V A and Uman M A 2003 *Lightning: Physics and effects* (New York: Cambridge University Press)

[38] Kochkin P O, van Deursen A P J and Ebert U 2014 Experimental study of the spatio-temporal development of metre-scale negative discharge in air *J. Phys. D: Appl. Phys.* **47** 145203

[39] Kostinskiy A, Syssoev V, Bogatov N, Mareev E, Andreev M, Bulatov M, Sukharevsky D and Rakov V A 2018 Abrupt elongation (stepping) of negative and positive leaders culminating in an intense corona streamer burst: Observations in long sparks and implications for lightning *J. Geophys. Res. Atmos.* **123** 5360–5375

[40] Albright N and Tidman D A 1972 Ionizing potential waves and high-voltage breakdown streamers *The Physics of Fluids* **15** 86–90

[41] Kirillov I, Rusanov V and Fridman A A 1985 On the diffusion-electrodynamic instability of ionization wave front (in russian) *Dokl. Akad. Nauk SSSR* **284** 1352–1355

[42] Sinkevich O 2003 Anode streamer branching *High Temperature* **41** 609–618

[43] Khodataevev K V 2012 Discharge processes in a stratosphere and mesosphere during a thunderstorm *Proc.of 50th AIAA Aerospace Sciences Meeting including the New Horizons Forum and Aerospace Exposition, 09 - 12 January 2012, Nashville, Tennessee, USA* pp AIAA 2012–0662

[44] Florescu-Mitchell A and Mitchell J 2006 Dissociative recombination *Physics reports* **430** 277–374

[45] Babaeva N Y, Tereshonok D V and Naidis G V 2016 Fluid and hybrid modeling of nanosecond surface discharges: effect of polarity and secondary electrons emission *Plasma Sources Science and Technology* **25** 044008

[46] Soloviev V, Krivtsov V, Shcherbanev S and Starikovskaia S 2016 Evolution of nanosecond surface dielectric barrier discharge for negative polarity of a voltage pulse *Plasma Sources Science and Technology* **26** 014001

[47] Zhu Y, Shcherbanev S, Baron B and Starikovskaia S 2017 Nanosecond surface dielectric barrier discharge in atmospheric pressure air: I. measurements and 2D modeling of morphology, propagation and hydrodynamic perturbations *Plasma Sources Science and Technology* **26** 125004

[48] Vasilyak L, Kostyuchenko S, Kudryavtsev N and Filyugin I 1994 High–speed ionization waves at an electric breakdown *Phys.–Uspekhi* **163** 263–286

[49] Kusyn L, Synek P B M M and Hoder T 2021 Remote streamer initiation on dielectric surface *Plasma Sources Sci. Technol.* **30** 03LT02

[50] Raizer Y P 1991 *Gas discharge physics* (Verlag Berlin Heidelberg: Springer) ISBN 978-3-642-64760-4

[51] Ferreira N G C, Naidis G V and Benilov M S 2021 Simulation of pre-breakdown discharges in high-pressure air: II. Effect of surface protrusions *Journal of Physics D: Applied Physics* **54** 255203

[52] Capitelli M, Ferreira C M, Gordiets B F and Osipov A I 2000 *Plasma Kinetics in Atmospheric Gases* (Berlin, Heidelberg: Springer)

[53] Soloviev V 2021 Surface discharges: possible applications for plasma-assisted ignition and electric field measurements *Proc.of 20th International Workshop on Magneto-Plasma Aerodynamics, Moscow, Russia, May 25-27, 2021*

[54] Smirnov B 1974 *Ions and excited atoms in plasma* (Atomizdat (In Russian))

[55] Chng T, Lepikhin N, Orel I, Popov N and Starikovskaia S 2020 Talif measurements of atomic nitrogen in the afterglow of a nanosecond capillary discharge *Plasma Sources Sci. Technol.* **29** 035017